Waveform-Controlled Relativistic High-Order-Harmonic Generation

Matthew R. Edwards and Julia M. Mikhailova

Phys. Rev. Lett. **117**, 125001 — Published 16 September 2016

DOI: 10.1103/PhysRevLett.117.125001

Waveform-Controlled Relativistic High-Order-Harmonic Generation

Matthew R. Edwards[1] and Julia M. Mikhailova[1,*]

[1]*Department of Mechanical and Aerospace Engineering, Princeton University, Princeton, New Jersey, 08544*

We consider the efficiency limit of relativistic high-order-harmonic emission from solid targets achievable with tailored light fields. Using one-dimensional particle-in-cell simulations, the maximum energy conversion efficiency is shown to reach as high as 10% for the harmonics in the range of 80-200 eV and is largely independent of laser intensity and plasma density. The waveforms most effective at driving harmonics have a broad spectrum with a lower frequency limit set by the width of the incident pulse envelope and an upper limit set by the relativistic plasma frequency.

Relativistic high-order-harmonic generation (HHG) using reflection from solid-density targets may provide a mechanism for the efficient production of high-intensity phase-locked extreme-ultraviolet and x-ray radiation [1–9], potentially allowing the exploration of new regimes in non-linear attosecond optics at intensities beyond the capabilities of gas-based HHG [10]. In the relativistic regime, over-dense-plasma HHG can be described by the coherent synchrotron emission model [11–13], in which, during each optical cycle, a dense bunch of electrons is coherently driven by the laser and plasma fields through an instantaneously synchrotron-like orbit, emitting a sub-femtosecond burst of intense high-frequency radiation. Despite advances in femtosecond technology to petawatt peak powers, relativistic HHG remains limited by on-target laser intensity, so methods to increase conversion efficiency at fixed intensity are critical. The efficiency of HHG, defined here as either the fraction of incident laser energy up-converted to particular high harmonics or the ratio of brightest attosecond pulse intensity to incident laser intensity, is strongly affected by laser intensity, target density, angle of incidence [14], and small density gradients on the target surface [15]. Both measures of efficiency depend directly on the rate at which harmonic intensity (I) decreases for increasing harmonic frequency (ω), with the applicability of various proposed scaling laws, e.g. $I(\omega) \propto \omega^{-8/3}$ [16] or $I(\omega) \propto \omega^{-4/3}$ [13], debated vigorously in the literature [12, 17–20]. With the aim of increasing HHG efficiency at fixed laser intensity, driving laser beams containing two [21–24] or more [25, 26] colors have been studied; recent results suggest that multiple-color beams can be substantially more effective than equivalent-energy single color beams across a broad range of conditions. To understand the predicted enhancement and effectively use recent advances in short-pulse waveform synthesis [27, 28], we comprehensively study manipulation of the driving waveform, finding a limit on the efficiency of relativistic HHG and demonstrating a method for reaching it.

The balance between the incident-laser light pressure and the space-charge field of the target plasma governs the behavior of solid-target relativistic HHG. The laser is characterized by its normalized amplitude ($a_0 = E_0/E_{\mathrm{rel}}$, where $E_{\mathrm{rel}} = m_e\omega_L c/e$, E_0 is the maximum electric field, ω_L is the laser frequency, and e and m_e are the charge and mass of an electron), and the strength of the plasma response is determined by its density ($N = n_e/n_c$ where $n_c = m_e\omega_L^2/4\pi e^2$ is the plasma critical density and n_e is the electron number density). The similarity parameter $S = N/a_0$, which arises from analysis of the Vlasov-Maxwell equations for $a_0 \gg 1$ [29], is key to describing HHG, because the electron dynamics at $a_0 \gg 1$ depend primarily on S rather than N or a_0 separately [16, 30]. The interaction physics may be moved to a more efficient regime by manipulating the laser frequency ($S \propto 1/\omega_L$) since for $a_0/N < 0.5$, common for current experiments, efficiency increases at higher frequencies [21]. However, gains from frequency doubling or tripling are limited, particularly if the objective is the generation of isolated attosecond pulses, because a frequency-doubled beam will contain twice as many optical cycles under its envelope.

Let us consider an incident laser with fixed fundamental frequency ω_L, of which an arbitrary energy fraction (W_n/W) is converted to other frequencies (ω_n) with specified relative phase (ϕ_n), under the constraint that the total beam must remain periodic with $T_L = 2\pi/\omega_L$. This allows arbitrary waveforms with period T_L and restricts us to harmonics of the fundamental frequency. Here we use a genetic algorithm to search the $(2n-1)$-dimensional space $[\phi_{1,\ldots n}, W_{2,\ldots n}]$ for $n \leq 20$ with particle-in-cell (PIC) simulations (EPOCH [31]), aiming to either maximize the intensity of attosecond pulses or the energy in high-frequency portions of the reflected spectrum ($\omega > 20\omega_L$); optimizing for either measure resulted in similar waveforms. To check for convergence to local minima, at each condition our optimization algorithm was run with 12 different initial populations for each n between 1 and 20. Since each optimization represents up to 5000 simulations in 50-200 member populations, every set of parameters was studied with 2×10^5 to 1.2×10^6 separate simulations. All reported optimization results use one-dimensional PIC simulations with a spatial resolution of $\lambda/600$ and between 20 and 200 particles in each cell, depending on the target density. At relativistic intensities ($> 2 \times 10^{18}$ W/cm^2), we may treat the plasma as pre-

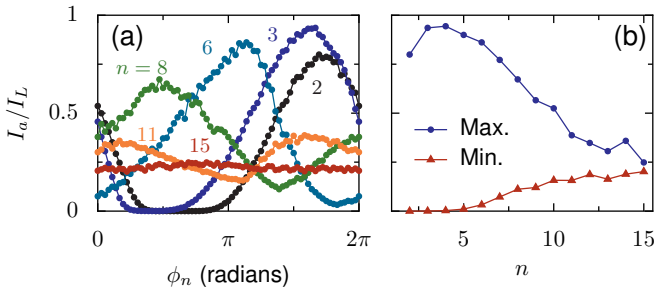

FIG. 1: (a) Attosecond pulse generation efficiency (I_a/I_L) for driving pulses with 10% of incident energy in the nth harmonic with phase ϕ_n. (b) Maximum and minimum generation efficiency achieved for varied ϕ_n at fixed n. Attosecond pulses are found by filtering the reflected spectrum so that $20 < \omega/\omega_L < 100$. For all points, $N = 400$, $a_0 = 40$, and $\theta_L = 30°$.

ionized, and for short laser pulses ($\tau < 20$ fs FWHM), the ions may be treated as immobile. Driving laser pulses at non-normal angles of incidence ($\theta_L > 0$) were p-polarized and, where not otherwise indicated, we used single cycle ($\tau = 3$ fs FWHM) pulses with fundamental wavelength $\lambda = 800$ nm.

Light at frequencies substantially above the plasma frequency ($\omega_p^2 = 4\pi n_e e^2/m_e$) will pass through the plasma front with little interaction, so high-frequency components ($\omega_n = n\omega_L$) should have a decreasing effect for increasing harmonic number n. At relativistic intensities ($a_0 \gg 1$), the effective plasma frequency (ω_{pR}) decreases due to the relativistic increase in electron mass ($\omega_{pR}/\omega_L = \sqrt{N/\gamma} \approx \sqrt{N/a_0}$), further reducing the highest frequency that will strongly interact with the plasma. Figure 1 demonstrates this for an incident waveform where 10% of the energy in the fundamental ($\lambda = 2\pi c/\omega_L = 800$ nm) frequency is converted to its nth harmonic, and the attosecond pulse generation efficiency ($\eta = I_a/I_L$, where I is the maximum intensity of (a) the attosecond pulse or (L) the incident laser) is measured for varied second-color phase (ϕ_n). As n increases to 15, both the maximum enhancement and maximum suppression (Fig. 1b) converge to the same value after reaching a maximum difference for n near ω_{pR}/ω_L (for the parameters in Fig. 1, $\omega_{pR}/\omega_L = 3.2$). This suggests that the optimized solution will be found for finite n of order ω_{pR}/ω_L, making the optimization problem tractable for the parameters of interest.

In contrast to gas-phase HHG, where the optimal waveform consists of a linear ramp and DC offset [32–34], the optimal waveforms for relativistic HHG are single oscillations of the electric field with an effective frequency directly related to the relativistic plasma frequency (Fig. 2). This holds true whether we consider single cycle (3 fs) or multi-cycle (15 fs) incident pulses. Figure 2 presents (a) optimized waveforms and (b) the corresponding reflected spectra for incident beams containing

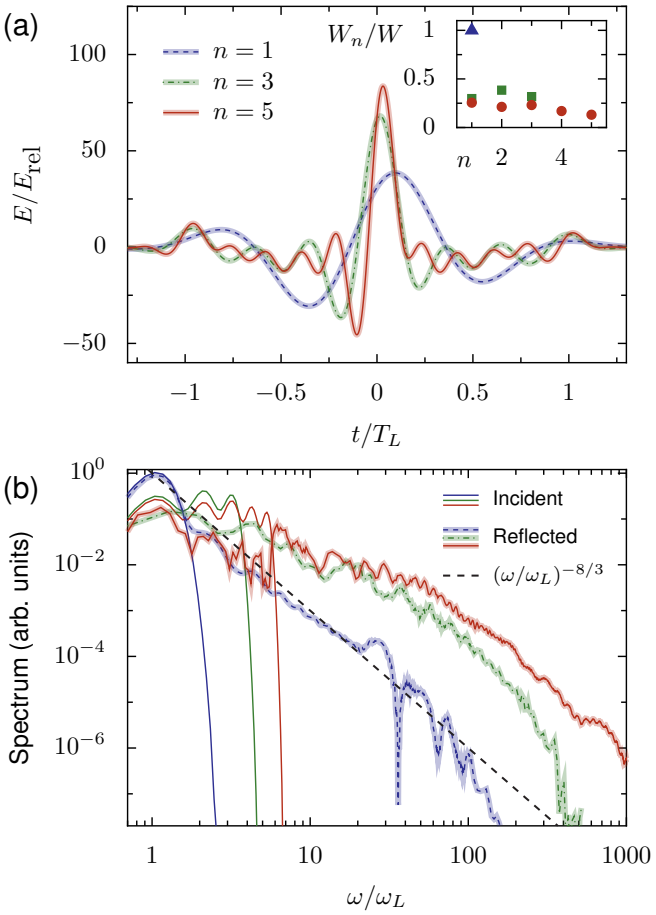

FIG. 2: (a) Optimal waveform at $N = 400$, $a_0 = 40$, and $\theta_L = 30°$ for $n = 1, 3, 5$. The $n = 5$ solution (fundamental and first four harmonics) is the global optimum, with no additional enhancements seen for including 6 or more frequencies. Inset: fraction of incident energy contained in each frequency. (b) Corresponding spectra of incident and reflected fields, with $\omega^{-8/3}$ scaling indicated for reference.

one, three, or five frequencies; for $a_0 = 40$ and $N = 400$, increasing n above five does not further increase η. The energy (inset, Fig. 2a) is distributed relatively equitably among the different frequencies for $n = 5$, highlighting the importance of both the low (ω_L) and high ($5\omega_L$) frequency components in building an optimal waveform.

The HHG efficiencies of optimized waveforms set a limit substantially higher than any efficiencies that have been previously demonstrated. For example, of the incident energy in the $n = 5$ optimized waveform in Fig. 2, 14% is absorbed by the plasma, 23% is reflected in the first five harmonics, and 63% is converted to higher frequencies ($\omega \geq 6\omega_L$). In comparison to previous PIC simulations which found up to 0.6% of the incident energy reflected in the 80-200 eV ($52 \leq \omega/\omega_L \leq 129$) zirconium filter range using a $L/\lambda = 0.25$ density gradient [35], for our optimized waveform this interval contains 10% of the incident energy. Manipulation of incident frequencies

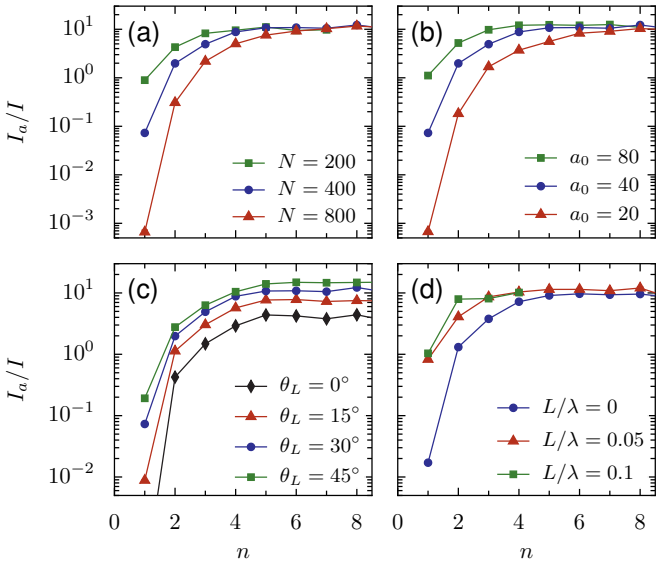

FIG. 3: Attosecond pulse generation efficiency (I_a/I) achieved with optimization over n frequencies. Where not otherwise noted, the simulation parameters are $N = 400$, $a_0 = 40$, $\theta_L = 30$, $L/\lambda = 0$, and $\tau = 3$ fs, and attosecond pulse intensity is calculated by filtering out frequencies lower than $20\omega_L$. Panels (a-d) show the effect of varying (a) N, (b) a_0, (c) θ_L, and (d) L/λ. In (d), $a_0 = 20$ and $N_{\max} = 200$.

may therefore allow far higher HHG efficiencies.

For different experimental parameters the optimized waveforms are qualitatively similar and give the same pulse generation efficiency (I_a/I_L). Variations in a_0, N and L/λ appear to change only the number of incident frequencies required to reach the optimal value, not the maximum value of the pulse generation efficiency (Fig. 3). From Fig 3a and b, the number of frequencies required required to produce an optimal waveform is approximately proportional to $\sqrt{N/a_0}$, which is consistent with the observation that incident frequencies substantially above the plasma frequency have little effect on HHG. In contrast to $n = 1$, where the efficiency of attosecond pulse generation varies with angle of incidence by orders-of-magnitude, Fig. 3c shows a slight dependence of optimized efficiency on angle of incidence (θ_L). The efficiency of HHG is also less affected by the exponential density gradient scale length (L/λ) for optimized waveforms. Taken together, the plots in Fig. 3 suggest that the maximum possible HHG efficiency is consistent over a wide range of initial conditions.

From a synchrotron model for attosecond pulse emission, the effective laser frequency seen by the driven electron bunches prior to emission is set by the time between the zero-crossing-point of the experienced field (near t_2) and the electron interaction with the field maximum (at t_3) [11, 25]. Since the displacement into the plasma for $a_0/N < 0.5$ tends to be small compared to the wavelength ($\approx \lambda/10$), we can neglect the effect of relativistic electron motion in calculating the effective frequency of the driving field. The inset of Fig. 4 shows the trajectory of an emitting electron bunch, with key times marked; an attosecond pulse is generated at t_3. Taking the time between t_2 and t_3 to be one quarter of the effective laser period [$T_{LE} = 4(t_3 - t_2)$], we can calculate an effective laser frequency ($\omega_{LE} = 2\pi/T_{LE}$), which, normalized by the laser fundamental frequency, forms the y-axis of Fig. 4. Comparison of ω_{LE} for optimal waveforms at different values of a_0 and N to the relativistic plasma frequency $\omega_{pR}/\omega_L \approx \sqrt{N/a_0}$ in Fig. 4 shows that the optimal waveform matches the timescales of the laser-driven and space-charge-driven motions. In the relativistic transparency regime ($N/a_0 \approx 1$), the fundamental frequency is higher than the relativistic plasma frequency, so the addition of higher harmonics is not advantageous and the relationship between ω_{LE} and $\sqrt{N/a_0}$ begins to break down. Note that the ω_{LE} often lies at approximately half the value of the highest frequency necessary for optimization.

The limits of waveform optimization are well visualized by plotting the optimal achievable efficiency (I_a/I_L) against a_0/N (Fig. 5). The highest gains due to waveform shaping are seen for $a_0/N < 0.5$, where even two-color driving beams ($n = 2$) can produce attosecond pulses two orders of magnitude more intense than comparable single-frequency beams. The frequency matching physics that underlie the shape of the optimized waveform are evidenced by the convergence of the n-frequency optimization lines (triangles) with the global optimum at smaller values of a_0/N for larger values of n. We must emphasize that to optimize the waveform it is not sufficient to use a single frequency beam with $\omega_L \approx \omega_{pR}$, i.e. $a_0 \approx N$. The factor-of-four gap between the maximum efficiency achieved with single frequency beams (circles) at $a_0/N \approx 0.5$ and the optimal efficiency there shows that additional component frequencies always provide some benefit. For all $a_0/N \leq 0.5$, the optimal driving waveform contains subcycle field transitions with an effective frequency of ω_{pR} and minimizes the total number of strong field features under the pulse envelope.

It is important to note that the fundamental frequency of the optimized waveforms contains a significant fraction of the energy. Since our analysis is normalized by ω_L, this suggests that for pulse envelopes longer than single cycle at ω_L it will be advantageous to also add lower-frequency light, phase-matched to produce a waveform with a single strong oscillation. This is also in agreement with the observation that longer driving pulses at fixed frequency will tend to produce lower maximum intensities due to disruption of the plasma surface by repeated strong interactions. Fig. 6 compares the attosecond pulse train produced by a 30 fs driving pulse containing only $\lambda = 800$ nm light with a pulse where $W_{0.5}/W = W_{0.25}/W = 0.1$, demonstrating that the addition of low frequencies results in a strong isolated attosecond pulse rather than a

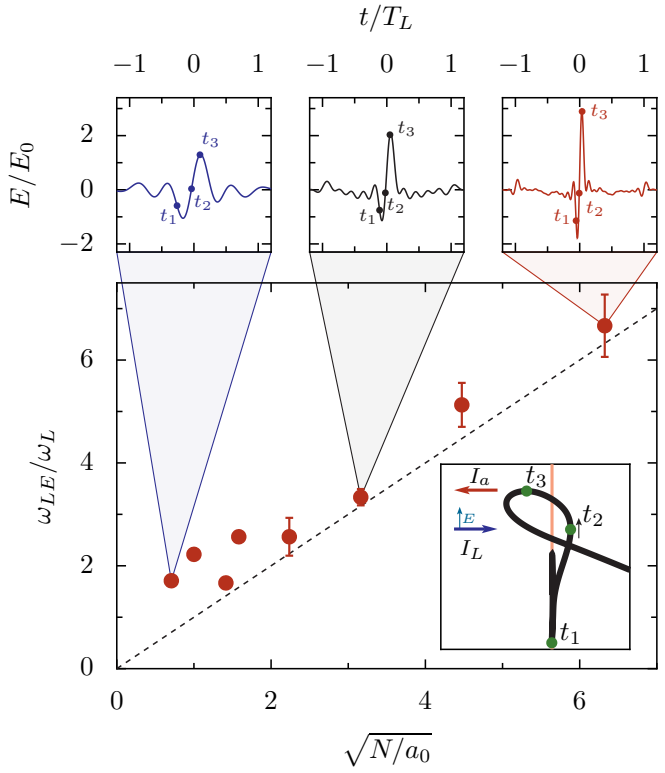

FIG. 4: Relativistic plasma frequency (dashed line) compared to the effective laser frequency (ω_{LE}) of optimal incident waveform for varied target density to laser amplitude ratio. The effective laser frequency is calculated by taking the time between the zero-crossing of the field at $t = 0$ (near t_2) and the maximum field intensity (at t_3) as one quarter of the effective laser period. Incident waveforms are shown for selected points at $N/a_0 = 0.5$, 10, and 40. The error bars indicate the range of effective frequencies calculated from waveforms producing within 5% of the maximum efficiency at those parameters. Inset: The trajectory of an emitting electron bunch for normal incidence geometry, with the ion positions marked by the vertical line and the laser incident from the left. Electrons begin near the center of the schematic, are pushed away from the ions between t_1 and t_2, and then turn before emitting at t_3.

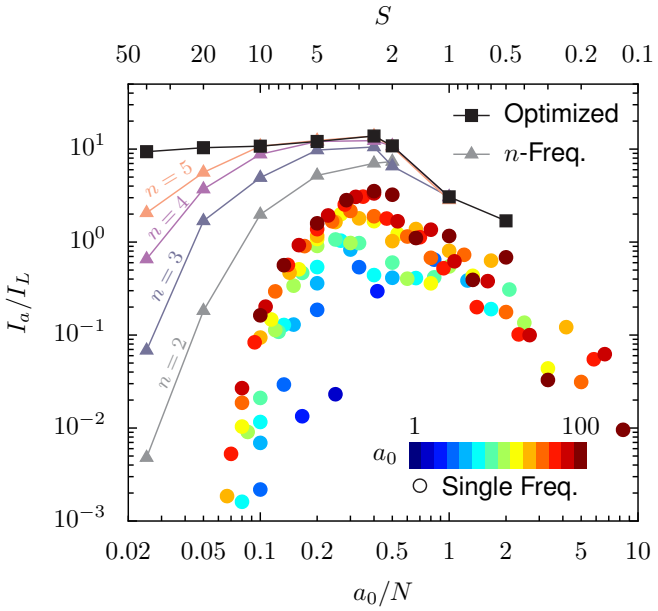

FIG. 5: Efficiency of attosecond pulse generation (filtered by $\omega/\omega_L > 20$) for optimized (black squares) and single frequency [$n = 1$] (circles) driving waveforms with varied a_0 and N at $\theta = 30^\circ$. The maximum efficiencies achieved with a restricted number ($n = 2$-5) of available frequencies (triangles) illustrates the number of harmonics required to build an optimal waveform as a function of a_0 and N.

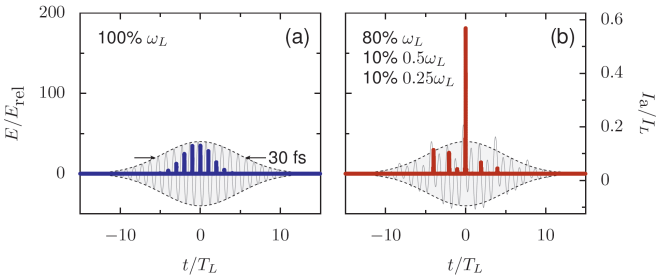

FIG. 6: Attosecond pulse trains (filtered by $10 < \omega/\omega_L < 100$) produced by 30 fs (FWHM, field) incident pulses at either (a) $\lambda = 0.8$ μm or (b) a mixture of 0.8, 1.6, and 3.2 μm light with $N = 400$, $a_0 = 40$, and $\theta_L = 30^\circ$. The left vertical axis is for the incident electric field (light gray) and its envelope, and the right axis is the scale for the attosecond pulse intensity.

train of weak pulses. The bandwidth required to produce an optimal waveform is set at its upper limit by the relativistic plasma frequency and at its lower limit by the duration of the pulse envelope; the addition of infrared light may therefore be advantageous for relativistic HHG.

Though current experimental systems are not capable of producing fully optimized pulses at the intensities discussed here, rapid progress in the development of broad bandwidth synthesized waveforms [27, 28], including multi-mJ multi-octave pulses [36] and the delivery of 80 mJ in 5 fs using two-color pumping for optical parametric chirped pulse amplification [37], suggests a path towards the experimental study of relativistic HHG with arbitrary waveforms.

In conclusion, we have found the maximum efficiency for relativistic high-order harmonic generation and demonstrated that it can be achieved through waveform control of the driving laser. The optimal waveform is constructed from a broad bandwidth with high frequencies to match the relativistic plasma frequency and low frequencies with period comparable to the pulse envelope duration. We show, for example, that when the reflected pulse is filtered to discard frequencies below $20\omega_L$, the remaining attosecond pulses may be up to ten times brighter than the incident pulse, with this limit depending only weakly on angle of incidence and not on laser

intensity or target density. At a 30° angle of incidence, 63% of the incident laser energy may be shifted above its initial bandwidth. This study provides an understanding of the waveform-shape dependence of HHG, finds the maximum efficiency of relativistic high-order harmonic generation, and suggests experimental paths towards enhanced relativistic HHG by combining the driving laser fundamental frequency with lower and higher frequency light.

This work was partially supported by the NSF under Grant No. PHY 1506372, and M.R.E. gratefully acknowledges the support of the NSF through a Graduate Research Fellowship. The presented simulations were performed at the High Performance Computing Center at Princeton University. The EPOCH code was developed as part of the UK EPSRC 300 360 funded project EP/G054940/1.

* Electronic address: mredward@princeton.edu, j.mikhailova@princeton.edu

[1] P. Gibbon, Phys. Rev. Lett. **76**, 50 (1996).
[2] R. Lichters, J. Meyer-ter Vehn, and A. Pukhov, Phys. Plasmas **3**, 3425 (1996).
[3] N. M. Naumova, J. A. Nees, I. V. Sokolov, B. Hou, and G. A. Mourou, Phys. Rev. Lett. **92**, 063902 (2004).
[4] Yu. M. Mikhailova, V. T. Platonenko, and S. Rykovanov, JETP Lett. **81**, 571 (2005).
[5] B. Dromey, S. Kar, C. Bellei, D. Carroll, R. Clarke, J. Green, S. Kneip, K. Markey, S. Nagel, P. Simpson, et al., Phys. Rev. Lett. **99**, 085001 (2007).
[6] N. Naumova, C. Hauri, J. Nees, I. Sokolov, R. Lopez-Martens, and G. Mourou, New J. Phys. **10**, 025022 (2008).
[7] U. Teubner and P. Gibbon, Rev. Mod. Phys. **81**, 445 (2009).
[8] P. Heissler, R. Hörlein, J. M. Mikhailova, L. Waldecker, P. Tzallas, A. Buck, K. Schmid, C. M. S. Sears, F. Krausz, L. Veisz, et al., Phys. Rev. Lett. **108**, 235003 (2012).
[9] P. Heissler, A. Barna, J. Mikhailova, G. Ma, K. Khrennikov, S. Karsch, L. Veisz, I. Földes, and G. Tsakiris, Appl. Phys. B **118**, 195 (2015).
[10] F. Krausz and M. Ivanov, Rev. Mod. Phys. **81**, 163 (2009).
[11] J. M. Mikhailova, M. V. Fedorov, N. Karpowicz, P. Gibbon, V. T. Platonenko, A. M. Zheltikov, and F. Krausz, Phys. Rev. Lett. **109**, 245005 (2012).
[12] D. an der Brugge and A. Pukhov, Phys. Plasmas **17**, 033110 (2010).
[13] B. Dromey, S. Rykovanov, M. Yeung, R. Hörlein, D. Jung, D. Gautier, T. Dzelzainis, D. Kiefer, S. Palaniyppan, R. Shah, et al., Nat. Phys. **8**, 804 (2012).
[14] A. A. Gonoskov, A. V. Korzhimanov, A. V. Kim, M. Marklund, and A. M. Sergeev, Phys. Rev. E **84**, 046403 (2011).
[15] F. Dollar, P. Cummings, V. Chvykov, L. Willingale, M. Vargas, V. Yanovsky, C. Zulick, A. Maksimchuk, A. G. R. Thomas, and K. Krushelnick, Phys. Rev. Lett. **110**, 175002 (2013).
[16] T. Baeva, S. Gordienko, and A. Pukhov, Phys. Rev. E **74**, 046404 (2006).
[17] T. J. M. Boyd and R. Ondarza-Rovira, Phys. Rev. Lett. **101**, 125004 (2008).
[18] A. Pukhov, T. Baeva, D. An der Brügge, and S. Münster, Eur. Phys. J. D **55**, 407 (2009).
[19] T. Boyd and R. Ondarza-Rovira, Eur. Phys. J. D **58**, 137 (2010).
[20] A. Pukhov and D. an der Brügge, Eur. Phys. J. D **58**, 139 (2010).
[21] M. R. Edwards, V. T. Platonenko, and J. M. Mikhailova, Opt. Lett. **39**, 6823 (2014).
[22] S. Mirzanejad and M. Salehi, Phys. Rev. A **87**, 063815 (2013).
[23] A. Tarasevitch, R. Kohn, and D. Von Der Linde, J. Phys. B **42**, 134006 (2009).
[24] A. Tarasevitch and D. von der Linde, Eur. Phys. J. ST **175**, 35 (2009).
[25] M. R. Edwards and J. M. Mikhailova, Phys. Rev. A **93**, 023836 (2016).
[26] P. Zhang and A. Thomas, Appl. Phys. Lett. **106**, 131102 (2015).
[27] O. Mucke, S. Fang, G. Cirmi, G. Rossi, S.-H. Chia, H. Ye, Y. Yang, R. Mainz, C. Manzoni, P. Farinello, et al., IEEE J. Sel. Topics Quantum Electron. **21**, 1 (2015).
[28] C. Manzoni, O. D. Mücke, G. Cirmi, S. Fang, J. Moses, S.-W. Huang, K.-H. Hong, G. Cerullo, and F. X. Kärtner, Laser Photon. Rev. **9**, 129 (2015).
[29] S. Gordienko and A. Pukhov, Phys. Plasmas **12**, 043109 (2005).
[30] T. Baeva, S. Gordienko, and A. Pukhov, Phys. Rev. E **74**, 065401 (2006).
[31] T. D. Arber, K. Bennett, C. S. Brady, A. Lawrence-Douglas, M. G. Ramsay, N. J. Sircombe, P. Gillies, R. G. Evans, H. Schmitz, A. R. Bell, et al., Plasma Phys. Contr. F. **57**, 113001 (2015).
[32] S. B. P. Radnor, L. E. Chipperfield, P. Kinsler, and G. H. C. New, Phys. Rev. A **77**, 033806 (2008).
[33] L. E. Chipperfield, J. S. Robinson, J. W. G. Tisch, and J. P. Marangos, Phys. Rev. Lett. **102**, 063003 (2009).
[34] S. Haessler, T. Balčiunas, G. Fan, G. Andriukaitis, A. Pugžlys, A. Baltuška, T. Witting, R. Squibb, A. Zaïr, J. W. Tisch, et al., Phys. Rev. X **4**, 021028 (2014).
[35] G. D. Tsakiris, K. Eidmann, J. Meyer-ter Vehn, and F. Krausz, New J. Phys. **8**, 19 (2006).
[36] F. X. Kärtner, in *CLEO* (Optical Society of America, 2015), pp. SF1M–1.
[37] L. Veisz, D. Rivas, G. Marcus, X. Gu, D. Cardenas, J. Mikhailova, A. Buck, T. Wittmann, C. M. S. Sears, S.-W. Chou, et al., in *CLEOPR 2013* (Optical Society of America, 2013), p. TuD2_3.